This is a repository copy of *A validated design methodology for a closed-loop subsonic wind tunnel*.

Article:

A Validated Design Methodology for a Closed loop Subsonic Wind Tunnel

John Kaiser Calautit [a,*], Ben Richard Hughes [a], Hassam Chaudhry [a], Lik Fang Sim [b]

[a] School of Civil Engineering, University of Leeds, Leeds, United Kingdom

[b] Department of Industrial and Mechanical Engineering, Qatar University, Doha, Qatar

Abstract

A systematic investigation into the design and simulation of flow parameters in a closed-loop wind tunnel was carried out using Computational Fluid Dynamics (CFD). The analytical model for estimating pressure losses were directed as input boundary conditions. Full-scale model of the entire wind tunnel was considered instead of the conventional approach, in which only test section flow is simulated. This allowed for optimisation of flow quality not only in the test section but also the flow in the entire circuit. Analysis of the guide vane configurations showed that test section flow quality was more affected by flow conditions in upstream than downstream sections. Hence, special attention must be given while designing the vanes at upstream turns particularly corners in line with the test section. Validation of the test section with block model showed that CFD was able to replicate wind tunnel measurements of velocity, turbulence intensity and pressure coefficient with error below 10%.

NOMENCLATURE

U	velocity magnitude (m/s)
I_u	turbulence intensity in streamwise (%)
X, Y, Z	Cartesian co-ordinates (m)
D_H	hydraulic diameter (m)
Re	Reynolds number
ρ	air density (kg/m^3)
v	kinematic viscosity (m^2/s)
Q	volume flow rate (m^3/s)
k	pressure loss coefficient
h	total head loss (m)
g	gravitational acceleration (m/s^2)
A	cross-sectional area (m^2)
ΔP	total pressure loss (Pa)
P	pressure (Pa)
P_o	total pressure (Pa)
P_s	static pressure (Pa)
θ_e	included angle (˚)
L	length (m)
W	width (m)
H	height (m)
K_s	roughness height (m)
C_{ks}	roughness constant
u'	turbulent velocity fluctuation standard deviation (m/s)
U_∞	freestream velocity (m/s)
u_i	velocity measurement at point i (m/s)
$\bar{u}$	average wind speed of all points (m/s)
c_p	air pressure coefficient

1. INTRODUCTION

Small scale wind tunnels are fast becoming a significant research apparatus used in aerodynamic investigations to study the effects of air moving past solid objects. The principle components of a wind tunnel includes the contraction, test section and diffuser section. The contraction section is used to ensure the uniform passage of flow into the test section. Small wind tunnels typically have contraction ratios between 6 and 9 [1]. The test section is the chamber in which observations and measurements are made and its shape and size is principally determined by the testing requirements. Diffusers are chambers that expand along their length, allowing fluid pressure to increase with decreasing fluid velocities [2].

The general aerodynamic objective for most wind tunnels is to obtain a flow in the test section that is as near as probable to a parallel steady flow with a uniform speed throughout the test section. Conversely, each design is restricted by constraints that include maximum cost, available space, and available knowledge [3]. The fundamental principles utilised in modelling low speed aerodynamic flows include mass conservation, force and motion relating to the Newton's Second Law and energy exchanges governed by the First Law of Thermodynamics. In considering low-speed flows, the assumption of incompressible flow is often adopted [3].

The majority of the small research tunnels are of the open-circuit category, since power consumption is not a considerable factor in overall construction expenditure. The second type is the closed-loop wind tunnel, in which air re-circulates through a closed loop and therefore is subject to directional variations. The advantage associated with this type of wind tunnel includes superior control over flow quality by corner turning vanes and screens [4].

In this work, a methodology for developing a closed-loop subsonic wind tunnel was outlined. The methods for calculating the pressure losses for the wind tunnel were defined. The study used Computational Fluid Dynamics (CFD) to evaluate the wind tunnel test section flow quality. For the purpose of validation, experimental tests were conducted. Furthermore, the authors evaluated the accuracy of replicating the flow characteristics for which the wind tunnel was designed using CFD simulation. The study aims to enhance knowledge in the field of using numerical simulation as a feasible technique in the design of closed-loop wind tunnels.

2. PREVIOUS RELATED WORK

Recent developments in computational methods have significantly increased the use of numerical models. The application of CFD in Aerodynamics and Wind Engineering has significantly increased in the past decade [5, 6, 7]. Numerical methods are often used jointly with physical experimentation such as wind tunnel studies for validation and assessment of data obtained by simulation. However, the use of CFD to support wind tunnel design has remained very limited and has been situated in other research areas [8, 10]. Several works on the evaluation of wind tunnel systems using numerical models are highlighted in this section.

Moonen et al. [8] established a methodology for numerically modeling the flow conditions in a closed-circuit low speed wind tunnel system. Steady-state and three-dimensional CFD simulations, using standard and realizable k–epsilon equations models, were carried out to determine the total pressure loss and flow rate in the test section. Grid sensitivity analysis was

performed to verify the grid independence of the simulation of results for both the cases. The study showed that the accuracy of the results from the full wind tunnel model simulation was 2-4 times better than the conventional CFD analysis of only the test section.

Gordon and Imbabi [9] used CFD to simulate the flow within critical sections of the closed-loop wind tunnel at the University of Aberdeen. The study aimed to reduce the overall cost and size of the wind tunnel, facilitate the use of alternative working fluids and at the same time maintain the high quality of the flow in the test section. The results showed that the CFD methods played a significant part in classifying the required modifications to achieve compact and cost effective wind tunnel design.

Moonen et al. [10] investigated the flow quality in the test section of a closed loop wind tunnel test using numerical analysis. The work established six corresponding indices for the evaluation of the three-dimensional flow quality in the test section. The study highlighted the effect of adding guide vanes and mesh screens in the contraction nozzle to improve the flow quality in the working section. The findings depicted that the vertical guide vanes reduced the skewness and angularity, yielding a higher quality flow while the horizontal guide vanes were found to have a slightly negative impact.

From the previous related work, different types of wind tunnels have been studied using numerical CFD analysis. The numerical simulation and experimental results demonstrated the importance of the use of CFD in assessing the performance of a wind tunnel system. The good correlation between both methods of analysis suggested that the CFD techniques in use were suitable for this study.

The objectives of the work included achieving a uniformity of mean air velocity and turbulence intensity in the test-section in line with 1 % and to have a test-section capable of having a blockage ratio of less than 5 % for most applications [8, 11]. Table 1 compares the general specifications and constraints of existing wind tunnel facilities and also summarises the target values of flow quality for the University of Leeds wind tunnel.

Table 1 General specification and constraints of existing subsonic wind tunnel facilities

	Politecnico di Milano [12]	SWJTU-3 [13]	UNNE [14]	IPT WT [15]	University of Leeds
Location	Como, Italy	Jiatong, China	Chaco, Argentina	Sao Paulo, Brazil	Leeds, UK
Circuit Type	Closed-loop	Closed-loop	Open	Open	Closed-loop
Application	Civil/Aero Eng.	Civil Eng.	Structural Eng.	Calibration	Civil Eng.
Test section (m)	13.8 x 3.8	22 x 4.5	2.4 x 1.8	0.5 x 0.5	0.5 x 0.5
Speed (m/s)	>14	1 - 16.5	-	2.5 - 20	2 - 15
$\Delta U/U$ (%)	$\pm$ 2	-	3	$\pm$ 0.5	$\pm$ 1
Turbulence I_u	< 2	< 1	< 1	< 0.45	< 1

3. WIND TUNNEL FACILITY

The closed-loop wind tunnel facility was developed at the School of Civil Engineering at University of Leeds (Figure 1a). The wind tunnel consisted of an overall plan length of 5.6 m with a test section of the height, width, and length of 0.5, 0.5, and 1 m. The tunnel operates as

closed-loop; air that passes through the test section is drawn back into the fan and recirculated into the test section repeatedly. Guide vanes are used to turn the air flow around the corners of the wind tunnel while minimising the turbulence and pressure loss. The contraction, diffuser, test section and two corners are located at floor level and the return legs set with the axial fan are positioned vertically above the test section. The closed-loop wind tunnel facility will be used for a wide range of applications including aerodynamic testing, study of flow patterns in and around buildings and ventilation systems, flow visualisation and also calibration of meteorology instrumentations. The small scale facility will provide essential information to guide design assessments and fundamental research. Furthermore, it will also be used to validate computational fluid dynamics methods. Hence the flow quality in the test section must meet the standards for wind engineering studies.
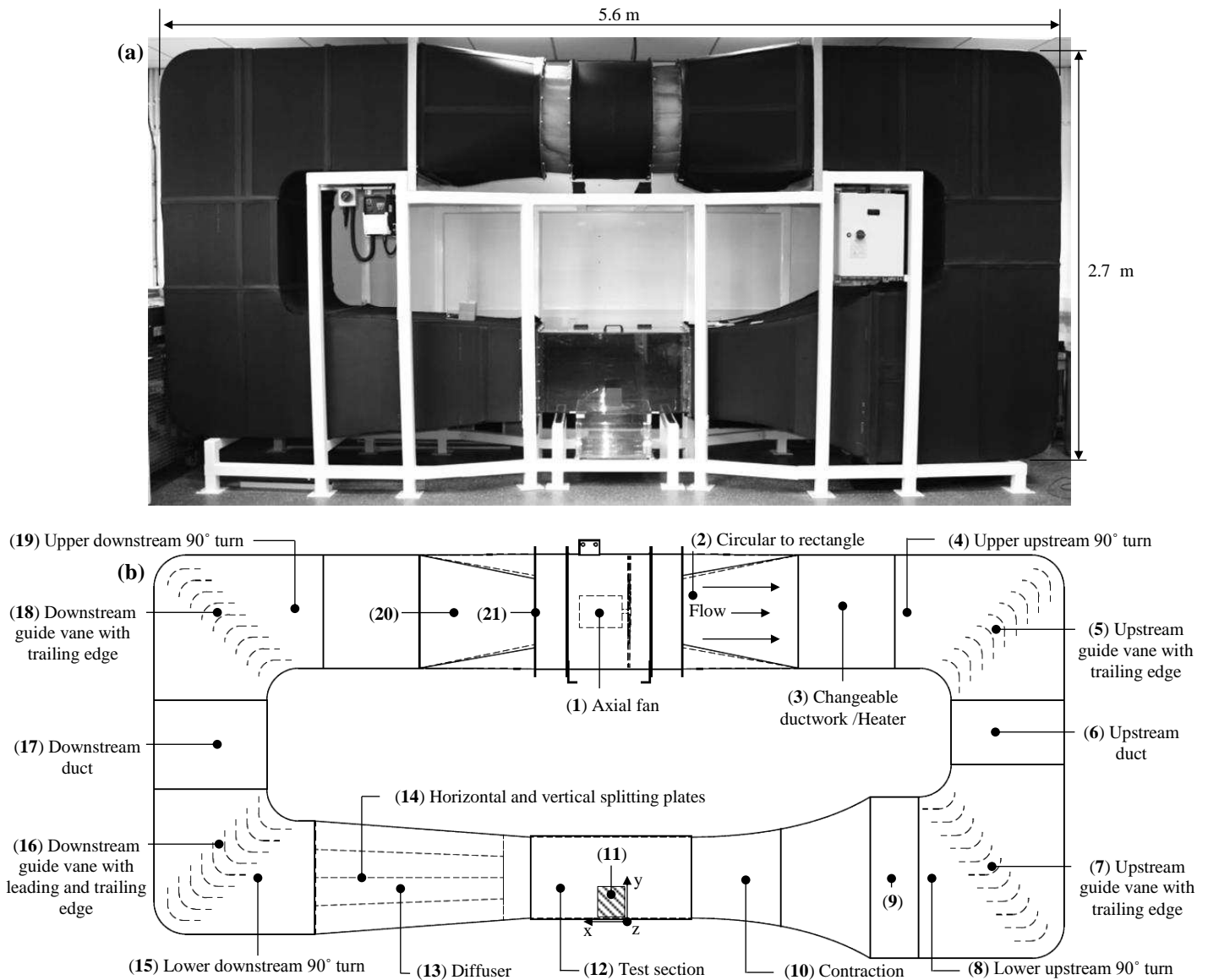

Figure 1 Side view of the (a) Final wind tunnel design (b) detailed CAD model of the closed-loop subsonic wind tunnel.

3.1. Mode of operation

A 0.7 m diameter 2.1 kW axial variable-revolution fan (**1**) drives the wind tunnel system (Figure 1b), it can create stationary wind flow within a range of 2 - 15 m/s. Behind the fan, is a smooth transition (**2**) of the cross-section from circular to a 1 x 0.7 m^2 rectangular duct (**3**). The neoprene circular to rectangle transition duct is used to reduce/absorb the vibration from the fan to the other wind tunnel components. In the 90˚ upstream section (**4**), 9 guide vanes (**5**) with 0.1 m extended trailing edges and 0.1 m spacing are located to reduce the flow separation occurring it the turn. The 0.4 m long upstream duct (**6**) connects the two upstream corners. A second set of guide vanes (11 vanes) with extended trailing edges (**7**) are positioned in the lower upstream 90˚ turn (**8**) forcing the flow to be parallel to the test section centre line and improved the uniformity of the flow before the contraction. A contraction section (**10**) with a 4:1 ratio and total length of 1.1 m connects the outlet of the settling chamber (**9**) to test section upstream. The 1 x 1 m^2 settling chamber will allow the integration of honeycomb and wire mesh for flow optimisation or adjustment of turbulence. Wind tunnel scale model (**11**) is positioned in the test section (**12**) which has a square cross-sectional area of 0.5 x 0.5 m^2 and a length of 1 m. Downstream of the test section is the diffuser section (**13**) which decelerates the flow in order to minimise the loss of flow kinetic energy. Particular effort is made to avoid flow separation in the diffuser, which can significantly reduce the overall performance of the wind tunnel [16-18]. In order to avoid these occurrences, 3 horizontal splitting plates with 0.25 m spacing and 3 vertical splitting plates with 0.17 m spacing (**14**) are installed inside the exit diffuser. The effect of the splitting plate was investigated by initial CFD simulations as show in Figure 2.
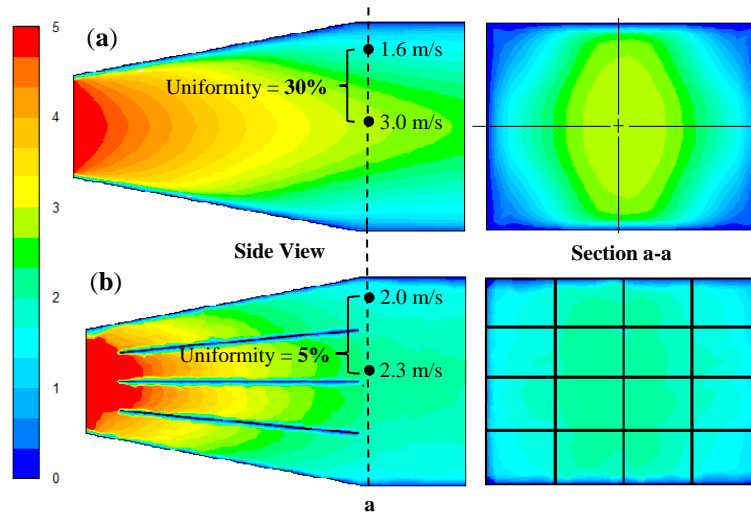

Figure 2 Comparison of flow in the wide angle diffuser: (**a**) without (**b**) with splitting plates.

Without the splitting plate (Figure 2a), the flow separation occurred at the downstream part of the diffuser. The separation was reduced significantly following the integration of the splitting plate (Figure 3b). This was evident from the uniformity of the flow field at the diffuser exit (velocity variation was reduced from 30 % to 5% following the addition of horizontal and vertical splitting plates). The downstream turn with guide vanes (**15, 16**) has a 1 x 1 m^2 square cross-section at the outlet of the diffuser, which gradually narrows to 1 x 0.7 m^2 rectangular cross-section at the downstream straight duct (**17**). In the 90˚ upper downstream section (**18**), 9 guide vanes (**19**) with 0.1 m extended trailing edges and 0.1 m spacing are located to order to

reduce the flow separation occurring in the turn. After the downstream, an abrupt transition of the cross-section from rectangular to circular cross-section (**20**) takes the flow into the fan. A highly porous safety mesh (**21**) is located at the end of the rectangle to round annular section to prevent models or parts entering the axial fan section and damaging the fan blades in case of model failure.

3.2. Total pressure loss

The power required to maintain steady flow through the wind tunnel is equal to the total losses occurring in the flow through the tunnel. The loss in kinetic energy, which appears as a decrease in total pressure, must be compensated by a pressure rise, in this case provided by the fan. Prior to conducting numerical simulations, the expected pressure loss for each section was determined. The pressure losses for all components of the wind tunnel were calculated in order to comprehend the functionality of the circuit [19]. The total pressure loss coefficients and head losses were obtained for upstream and downstream wind tunnel sections` alongside the corner vanes which are summarised in Table 2. The total head loss for the wind tunnel was calculated at 13.35 m providing a total pressure loss of 140.1Pa.

Table 2 Summary of the design specification, loss coefficient and pressure head loss of the wind tunnel sections.

Wind tunnel section	Description of component	Relevant loss coefficient /pressure formula	Loss coefficient	Head loss (m)
Contraction	Contraction ratio of 4:1, 1 m x 1 m (inlet) / 0.5 m x 0.5 m (exit) and 1.3 m (length)	$\Delta P = \frac{1}{2}\rho v_{in}^2\left[\left(\frac{A_{in}}{A_{out}}\right)^2 - 1\right]$	-	$\frac{P}{\rho g} = 3.97$
Test-section	Square test section, cross-sectional dimensions of 0.5 m x 0.5 m and length of 1 m.	$k = 1 - \frac{A_{specimen}}{A_{test}}$	0.91	$k \times \frac{u^2}{2g} = 4.64$
Diffuser	Diffuser area ratio of 3:1 and the included angle of 8° and 4°.	-	0.45	$k \times \frac{u^2}{2g} = 0.24$
Corners	90˚ bend	-	1.00	$k \times \frac{u^2}{2g} = 0.35$
Horizontal and vertical duct	Rectangular 1 m x 0.7 m duct	-	1.00	$k \times \frac{u^2}{2g} = 0.54$
Annular inlet	0.7 m diameter (fan) to 1 m x 0.7 m rectangular duct	$k = \frac{1}{AR^2} - 1 + k_d$	0.09	$k \times \frac{u^2}{2g} = 0.05$
Annular outlet	1 m x 0.7 m rectangular duct to 0.7 m diameter (fan)	$\Delta P = \frac{Q^2\rho\left[1 - \frac{A_2^2}{A_1}\right]}{2A_2^2}$	-	$\frac{P}{\rho g} = 0.94$

4. NUMERICAL METHODOLOGY

The commercial ANSYS Fluent numerical code was used for predicting the flow characteristics inside the closed-loop subsonic wind tunnel. The analytical model for estimating the pressure losses was directed as "intake fan" boundary conditions of the CFD model. A uniform boundary condition of the calculated pressure was imposed along the inlet surface (intake fan) and the outlet (pressure outlet) was set to zero gauge pressure. Two sets of simulations were conducted: numerical modelling of the wind tunnel with an empty test section and with a test block model located centrally in the test section. As suggested by Moonen et al. [8], a full-scale CFD model

of the entire wind tunnel was considered instead of the conventional approach, in which only the flow in the test section was modeled. The established CFD method accounted for the influence of the specific features of the wind tunnels such as guide vanes and splitting plates. This allowed for the optimisation of the flow not only in the test section but also the flow in other wind tunnel sections. Moreover, the "conventional approach" was not suitable for designing new wind tunnels as it requires experimental data to simulate the test section inlet boundary conditions and was only useful for studying existing wind tunnel systems.

During the design stage, four different wind tunnel configurations were investigated. The first model was the reference configuration in which no guide vanes were present. This configuration was compared to three others: with only guide vanes at the upstream, only guide vanes at the downstream and combined upstream and downstream guide vanes, correspondingly. The study evaluated the influence of the presence of guide vanes on the test section's flow quality (uniformity of the velocity flow field, flow angularity and turbulence intensity). Detailed investigation of the performance of the guide vane such as shape, chord length and curvature was outside the scope of the study.

4.1 Computational Mesh

The work combined the advantages of a structured with those of an unstructured grid to minimise the computational expense [8]. Sections of the wind tunnel that were of simple geometry in which one-dimensional flow dominates were meshed with structured prismatic mesh. In the sections of complex geometry with three-dimensional flows such as the diffuser, contraction and in the areas of the guiding vanes, tetrahedral/hybrid cells were used. The patch independent mesh algorithm was used. The method is based on the subsequent spatial subdivision algorithm which ensures refinement of the mesh where essential, but retains larger elements where feasible, therefore allowing faster computing times. It uses a top down meshing approach; the volume mesh is created first, and this is projected on to the faces and edges to generate the surface mesh. The approach is best for CAD models with many surfaces patches and with large number of small edges or sharp corners.

The grid resolution was determined taking into account an acceptable value for the wall Yplus with an average value of 222.3 for the wall-bounded cells. The average equiangle and equivolume skewness of the cells were 0.38 and 0.39 [20]. The complete meshed model comprised of 4,245,896 elements. A very high mesh resolution was applied at the walls of the turning vanes at all four corners in order to increase the accuracy of capturing the flow passing through. Figure 3 displays the details of the mesh for the corner guide vanes and diffuser splitting plates.

Table 3 indicates the type of mesh used and the total number of elements for different sections of the wind tunnel.
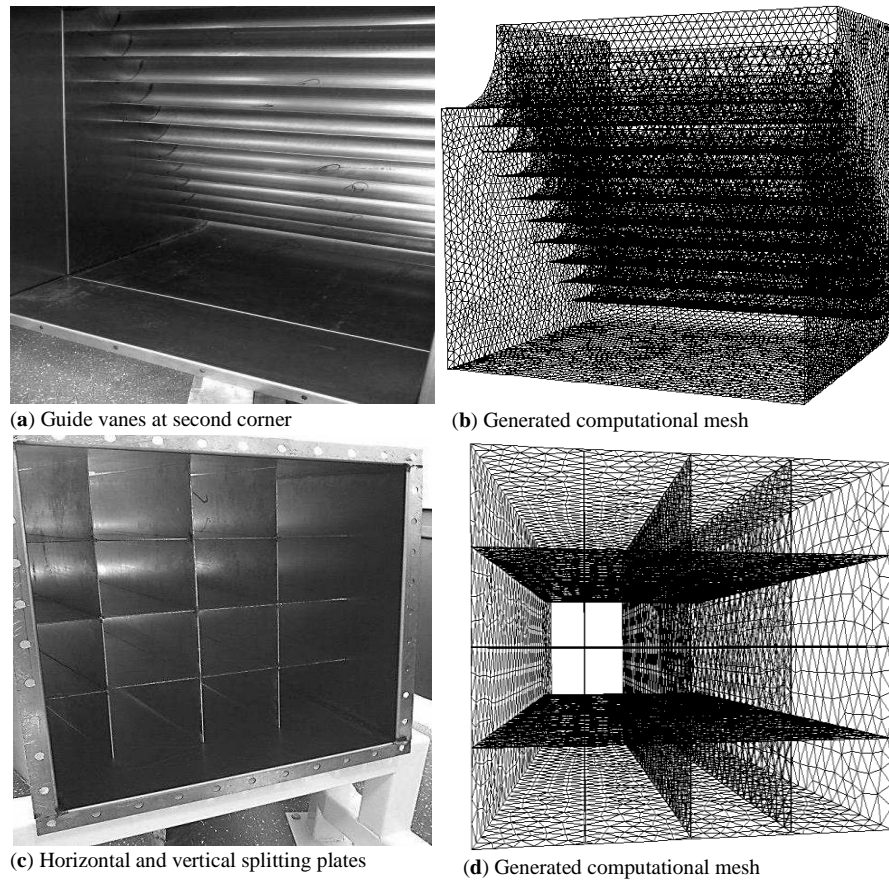
(**a**) Guide vanes at second corner

(**b**) Generated computational mesh

(**c**) Horizontal and vertical splitting plates

(**d**) Generated computational mesh

Figure 3 Actual photo of: (a) second corner guide vanes (b) diffuser exit. View of the computational mesh at the surface of: (c) the 90 corner guide vanes; (d) the diffuser splitting plates.

Table 3 Type and distribution of grid in the wind tunnel

Wind tunnel section	Grid Type	Number of elements
First corner	Tetrahedral	474,590
Upstream and downstream horizontal duct	Prismatic	351,967
Upstream and downstream vertical duct	Prismatic	297,213
Second corner	Tetrahedral	509,508
Contraction	Tetrahedral	452,131
Test-section (Empty)	Hybrid	636,884
Diffuser with splitting plates	Tetrahedral	559,508
Third corner	Tetrahedral	489,508
Fourth corner	Tetrahedral	474,590

4.2 Solution Methods

The three-dimensional Reynolds-averaged Navier-Stokes (RANS) equations and the continuity equation were solved using the commercial CFD code that employs the control-volume technique and the Semi-Implicit Method for Pressure-Linked Equations (SIMPLEC) velocity-pressure coupling algorithm with the second order upwind discretisation as recommended in literature [8]. Standard k-epsilon model was used primarily for the numerical simulation [7, 10].

The results obtained using the k-epsilon model were later compared with other turbulence models and experimental data. These included the k-e Renormalization Group (RNG) turbulence model [8], the k-w Standard and Shear-Stress Transport (SST) model and the Reynolds-Stress Model (RSM) with Linear Pressure-Strain and Stress-Omega models. The governing equations will not be repeated here but are available in [21]. Table 4 summarises the CFD model boundary conditions.

Table 4 Summary of the CFD model boundary conditions

Parameter	Set value
Discretisation Scheme	Second-order upwind
Algorithm	SIMPLEC
Time	Steady State
Intake fan (total pressure)	140.1 Pa
Pressure outlet	0 Pa
Gravity	-9.81

Furthermore, the walls, floor and ceiling, guide vanes and test section were modelled as solid walls with a set roughness height and constant. For the floor, side walls, ceiling and guide vanes, the physical roughness height was set to 0.015 (10^{-3}m). For the test section a roughness height of 0.0015 (10^{-3}m) was used. For all the surfaces, the roughness constant 0.5 was used [8, 22].

4.3 Grid Sensitivity Analysis

To investigate the solution independency from the grid several meshes were generated. Grid sensitivity analysis was used to validate the programming and computational operation of the computational model. The numerical grid was refined and locally enriched using the hp-method grid adaptation technique [23]. This procedure of evaluation requires the use of different mesh sizes (Meshes ranging from 1,622,108 to 7,149,235 elements) by the use of a posterior error estimates. The grid was evaluated and refined until the posterior estimate error becomes insignificant between the number of nodes and elements, computational iterations and the posterior error indicator [24, 25]. The maximum error for average velocity was recorded at 4.38%. The discretisation error was found to be the lowest at over 7 million cells for the indicated variable. The applied boundary conditions were remained fixed throughout the simulation process to ascertain precise comparison of the posterior error estimate.

5. WIND TUNNEL EXPERIMENTATION AND TESTING

Two sets of experiments were conducted: measurements in the wind tunnel with empty test section and with a block building model located centrally in the test section.

5.1 Empty wind tunnel test section

Complete characterisation of wind tunnel test environment is a massive task due to the very extensive range of achievable configurations including scaled model testing. Therefore, initial testing should be conducted with an empty test section [8]. The experiment comprised of measuring air velocities, pressure and turbulence intensity inside the empty test-section. Wind speed measurements were performed along 9 vertical lines located in the test-section (P01 –

P09), at intervals of 0.25m (horizontal) and 0.125 m (vertical). Table 5 summarises the coordinates of the measurements points.

Table 5 Summary of the measurement coordinates

Points	X [m]	Z [m]	Y [m]
P01	0.750	0.375	0 - 0.500
P02	0.500	0.375	0 - 0.500
P03	0.250	0.375	0 - 0.500
P04	0.750	0.250	0 - 0.500
P05	0.500	0.250	0 - 0.500
P06	0.250	0.250	0 - 0.500
P07	0.750	0.125	0 - 0.500
P08	0.500	0.125	0 - 0.500
P09	0.250	0.125	0 - 0.500
A	0.250	0.250	0.110
B	0.425	0.300	0.110
C	0.425	0.250	0.110
D	0.425	0.200	0.110
E	0.500	0.330	0.110
F	0.425	0.250	0.055
G	0.575	0.250	0.110

Since wind tunnel flow quality can adversely affect experimental results, precise and steady flow quality measurements are essential, along with the understanding of the causes and characteristic of flow turbulence in the wind tunnel. The instrumentation used in the measurements and characterisation of wind tunnel are summarised in Table 6. The measurements will provide comprehensive velocity, pressure and turbulence data that are vital to the assessment of the flow quality. The measurements were recorded when the temperature of the wind tunnel became stabilized at an ambient temperature of 298 K.

Table 6 Flow field quality measurement and measurement devices

Measurement	Method/Measurement points	Instruments	Relevant equations	Uncertainties
Velocity (m/s)	The velocity was measured at P01 - P09 (empty test section) and points A - G (with block model).	Testo 425, Hot-wire sensor [26]	-	$\pm$ 0.5 % rdg. at higher speeds (8 − 20 m/s)
Pressure (Pa)	The pressure was measured at points P01 - P09.	DPM ST650 with 166T ellipsoidal Pitot-static tube [27]	$P_o - P_s = \dfrac{1}{2}\rho U^2$	$\pm$ 1.0 % of reading at 22˚C, valid angle: $\pm$ 11˚
Turbulence intensity (%)	P01 - P09 (empty test section) and points A - G (with block model.	Testo 425, Hot-wire sensor [28]	$I = \dfrac{u'}{U_\infty}$	$\pm$ 0.5 % rdg. at higher speeds (8 − 20 m/s)
Flow uniformity	The mean flow uniformity was measured at points P01 - P09.	Testo 425, Hot-wire sensor [8]	$\mu_i = \dfrac{u_i}{\bar{u}} - 1$ [15]	$\pm$ 0.5 % rdg. at higher speeds (8 − 20 m/s)
Surface pressure coefficient	15 pressure taps located on the block model surfaces .	DSA3217 Pressure sensor and Pitot-static tube	$c_p = \dfrac{P - P_s}{\dfrac{1}{2}\rho U_{ref}^2}$ [29]	-

5.2 Wind tunnel test section with block model

The second experiment included velocity and turbulence intensity measurements around a test block model of the length, width and height of 0.11 m x 0.11 m x 0.11 m located centrally in the test section (Figure 4a). The model was furnished with 15 pressure taps located inside the model (See Figure 4b). The mean velocity and turbulence intensity profiles of the wind flow were measured using the hot-wire anemometer. The reference velocity, static and dynamic pressure were monitored using the pitot and static tubes mounted at the roof height of the block model. Figure 4c shows the test setup inside the test section. The surface pressure was transmitted to a Scanivalve digital pressure transducer, a sixteen channel DSA3217 digital sensor array, through the 0.002 m outside diameter tubulations. Each channel has its own temperature compensated piezoresistive pressure sensor. The unit contains a 16 bit A/D converter and it communicates data to DSAlink3 via Ethernet connection. The data were acquired at a sampling rate of 1000 samples/sec. For each pressure tap, 5 records of the pressure data, each comprising of 1,000 data points, were acquired.

The purpose of this test was to evaluate the accuracy of simulating or achieving the flow characteristics for which the wind tunnel was designed. According to the dimension of the model and wind tunnel cross-section, the model produces a maximum blockage of 5%, and no corrections were made to the pressure measurements obtained with this configuration [30, 31]. The values of the velocity and turbulence intensity were obtained from the three components of the vector (X, Y, Z). Table 5 summarises the coordinates of the measurements points for the experimental setup.
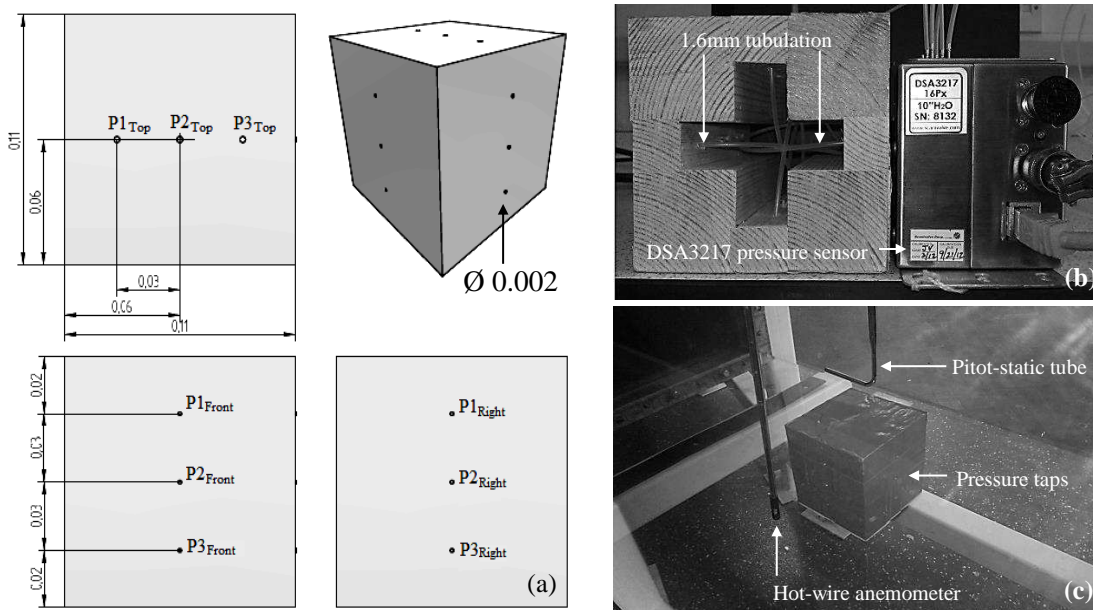
Figure 4 (a) Pressure tap locations on the square block model. (b) Internal view of the block model showing the 15 pressure taps connections. (c) Test setup: block model inside the test section. Dimensions in meters.

6. RESULTS AND DISCUSSION

6.1 Empty test section

Four different wind tunnel configurations were investigated. The first model was the benchmark configuration in which no guide vanes were present. This configuration was compared to three others: with only guide vanes at the upstream, only guide vanes at the downstream and combined upstream and downstream guide vanes, correspondingly. The study evaluated the influence of the presence of guide vanes on the test section flow quality. The quantities presented were, total velocity and pressure variation, a measure of the streamwise flow uniformity over the measurement area, the flow angularity, a measure of how parallel the flow is and the turbulence intensity.

6.1.1 Benchmark case: no guide vanes

The result in Figure 5 displays the air velocity profile inside the wind tunnel with no guide vanes at an inlet pressure of 140 Pa; the velocity variation within the test section was 1.44 %. The velocity between the test section and lower upstream turn increased to 16.27 m/s highlighting an increase factor of approximately 3. The unsteady flow in the test section can be observed which was caused by the flow separations in the upstream and downstream side of the wind tunnel corners.
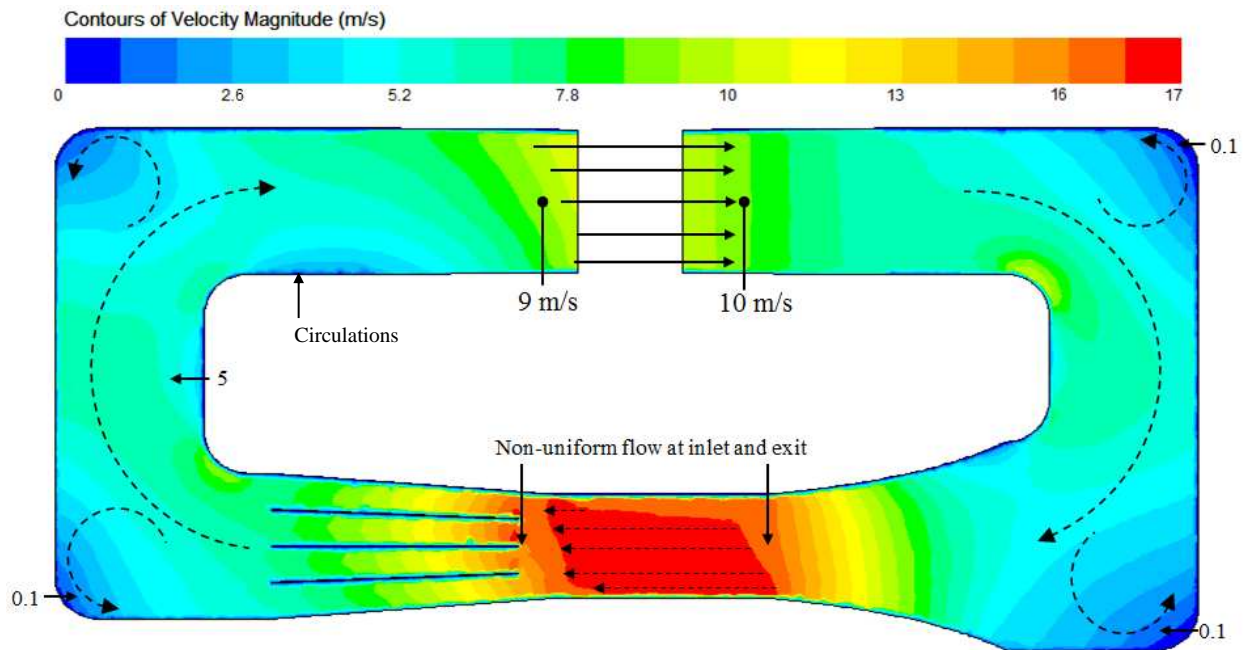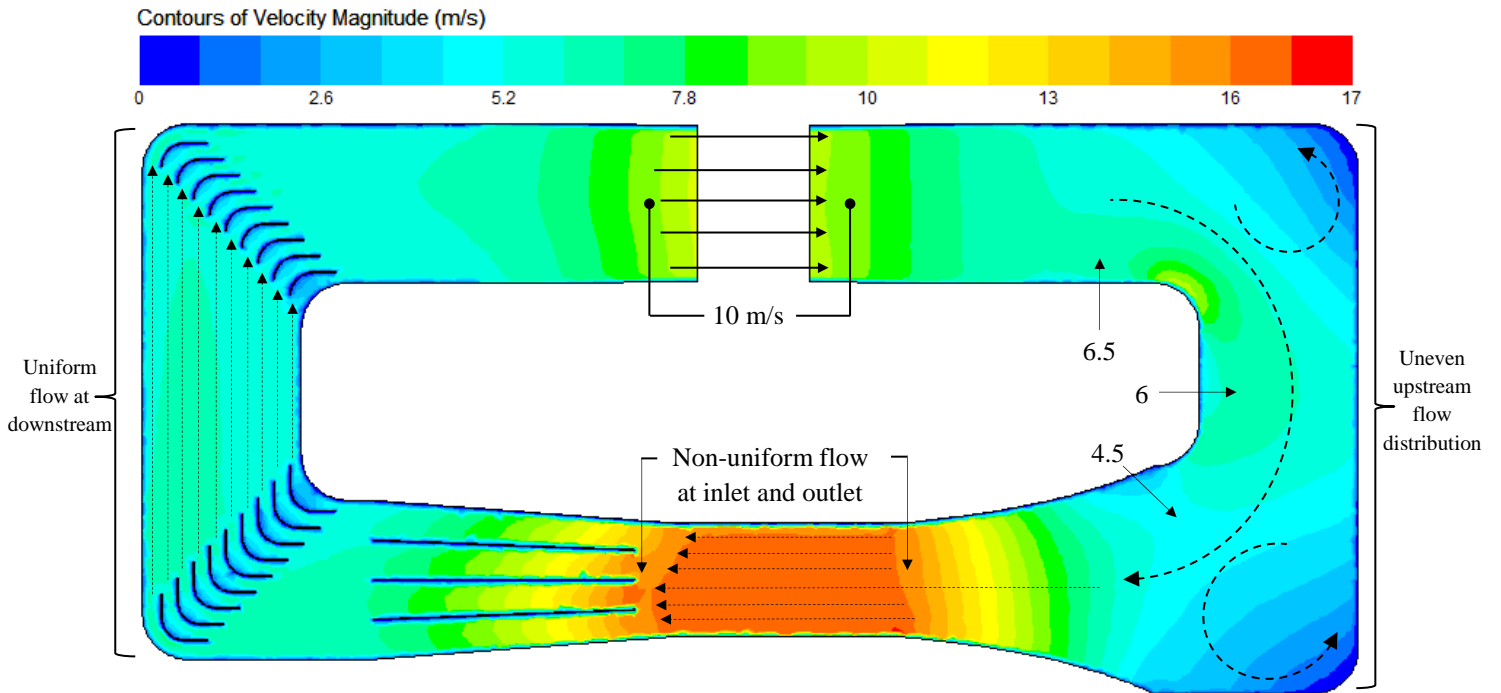

Figure 5 Contours of velocity magnitude for configuration 1: no guide vanes.

6.1.2 Upstream guide vanes

Figure 6 displays the flow profile inside the wind tunnel with upstream guide vanes, the velocity variation within the test section was lower (0.92 %) as compared to the benchmark case. As expected, average velocity in the test section was reduced to 15.97 m/s following the integration

of the guide vanes. Guide vanes in the upstream section significantly reduced the flow separations at the upper and lower corners. The air flow entering the test section was more uniform and symmetrical. However, it was seen that the velocity profile was not stable; it changes along the length of the test section. A highly disturbed flow was observed at the downstream due to up-flow present at the upper part of the test section outlet. Large flow separation at the exit of the test section was observed which was caused by the unsteady flows in the downstream corners. Furthermore, no improvement in the flow conditions was observed at the downstream side of the wind tunnel.
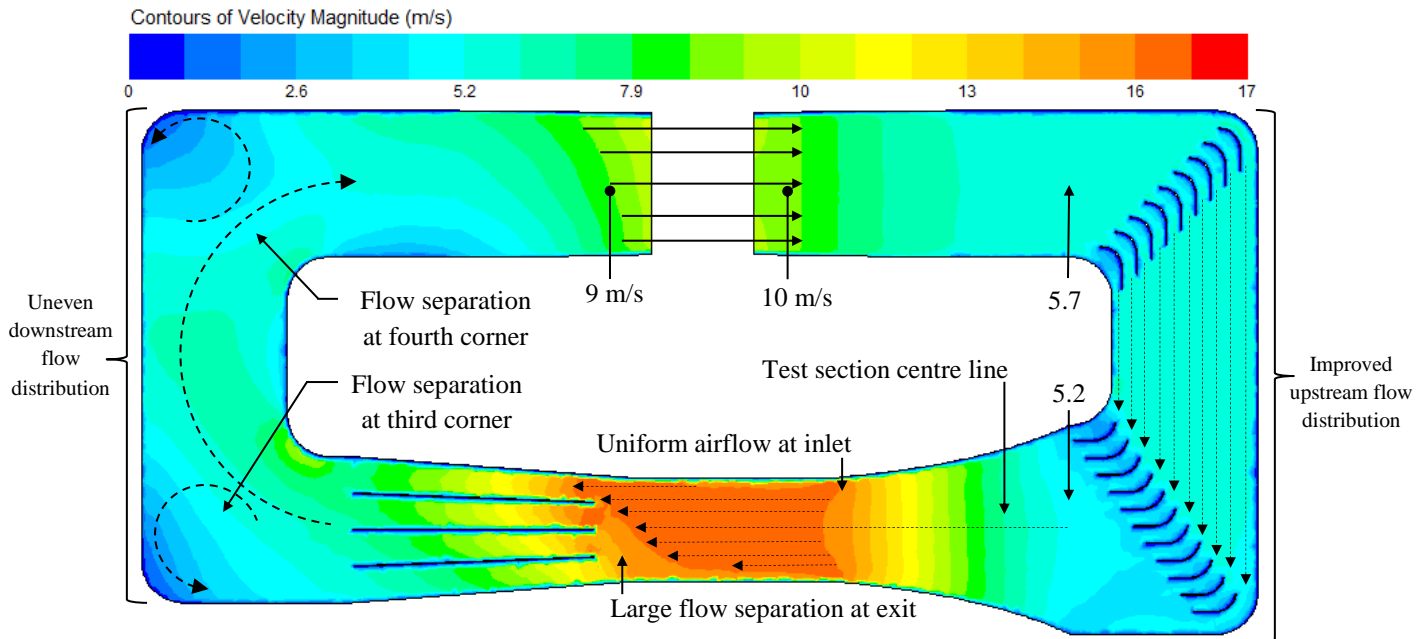
Figure 6 Contours of velocity magnitude for configuration 2: upstream guide vanes.

6.1.3 Downstream guide vanes

Figure 7 displays the flow profile inside the wind tunnel with downstream guide vanes, the velocity variation within the test section was higher (1.28 %) as compared to the configuration 2 with upstream guide vanes. Guide vanes in the downstream section significantly minimised the flow separations and circulations at the upper and lower corners. However, the improvement in the test section airflow uniformity due to the addition of downstream guide vanes was not significant compared to first configuration (upstream guide vanes). This shows that the uniformity of the airflow in the test section was more dependent on the flow quality at the upstream section of the tunnel. Hence, first two upstream corners were critical in terms of obtaining a uniform airflow in the test section especially the section in line with its centre line.

Figure 7 Contours of velocity magnitude for configuration 3: downstream guide vanes.

6.1.4 Upstream and downstream guide vanes

Figure 8 displays the flow profile inside the wind tunnel with the combined upstream and downstream guide vanes, the velocity variation within the test section was significantly lower (0.61 %) compared to other configurations. Average velocity in the test section was reduced to 15.85 m/s following the integration of the guide vanes in all corners. As expected, a more symmetric uniform flow was observed throughout the entire test section length and good overall airflow distribution in the wind tunnel circuit.
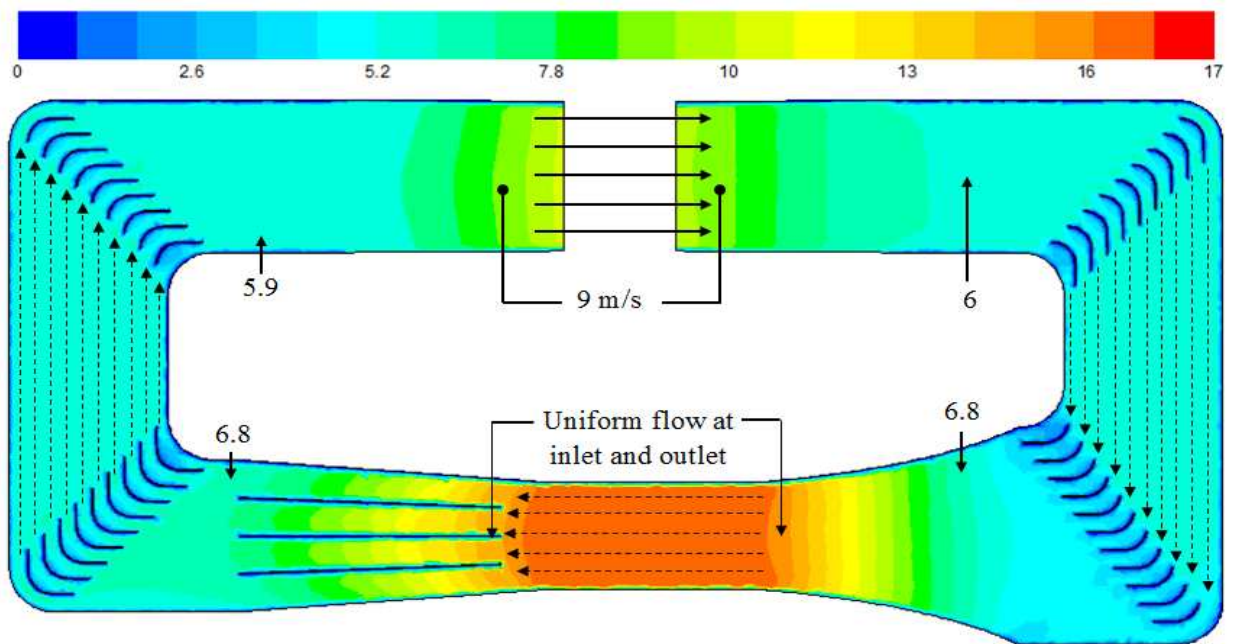
Figure 8 Contours of velocity magnitude for configuration 4: upstream and downstream guide vanes.

Table 7 summarises the velocity profile inside the test section for the guide vane configurations.

Table 7 Summary of velocity flow distribution in test section for the different guide vane configurations (vertical cross section)

	Vertical cross section (Z = 0.25 m)	Data
(a) No guide vanes		Average speed: **16.27 m/s**
(b) Upstream guide vanes		Average speed: **15.97 m/s**
(c) Downstream guide vanes		Average speed: **16.07 m/s**
(d) Upstream and downstream		Average speed: **15.85 m/s**

Table 8 summarises the velocity profile inside the test section for the guide vane configurations.

Table 8 Summary of velocity flow distribution in test section for the different guide vane configurations (horizontal cross section)

	Horizontal cross section (Y = 0.25 m)	Data
(a) No guide vanes		Average speed: **16.27 m/s**
(b) Upstream guide vanes		Average speed: **15.97 m/s**
(c) Downstream guide vanes		Average speed: **16.07 m/s**
(d) Upstream and downstream		Average speed: **15.85 m/s**

6.1.4.1 Velocity profile and turbulence intensity

The results in Figure 9 show the vertical wind speed profiles and turbulent intensity profiles at position P06 (0.25 m away from the inlet) of the test section for the different guide vane configurations. The wind speed values were made dimensionless by division by the reference velocity (maximum velocity across the vertical profile). Turbulence shows values around 1 % (configuration 2 and 4) and below 2.5 % (configuration 1 and 3) outside the boundary layer increasing inside the boundary layer. Good correlation was observed between the measured and CFD velocity and turbulence intensity profiles for configuration 4 (upstream and downstream guide vanes). Although, the measured points slightly deviates away from the CFD profile below 0.1 m and above 0.4 m of the test section.
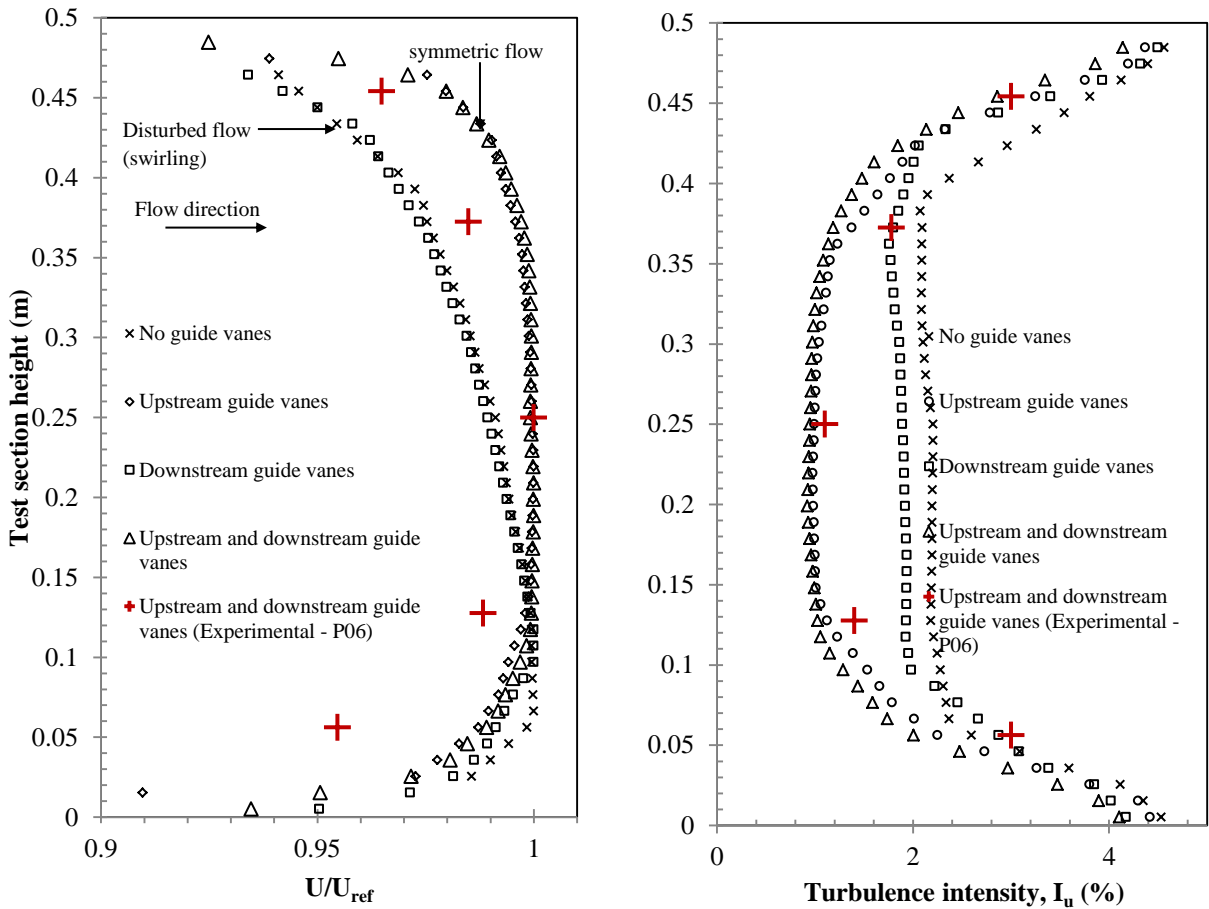
Figure 9 Comparison between the dimensionless mean velocity and turbulence intensity of the flow at the test section for the different wind tunnel configurations (**X = 0.25 m, P06**). Highlighted (**red**) data points show measured wind tunnel values.

The results in Figure 10 shows the vertical wind speed profiles and turbulent intensity profiles at position P04 (0.75 m away from the inlet) of the test section for the different guide vane configurations. The second configuration with only the upstream guide vanes did not maintain the uniformity of the flow near the outlet while, configurations 1 and 3 still showed a skewed flow. A symmetric flow profile was observed for the wind tunnel with the combined upstream and downstream guide vanes. Hence, it can be concluded that the flow quality was uniform throughout the entire length of the test section for configuration 4.
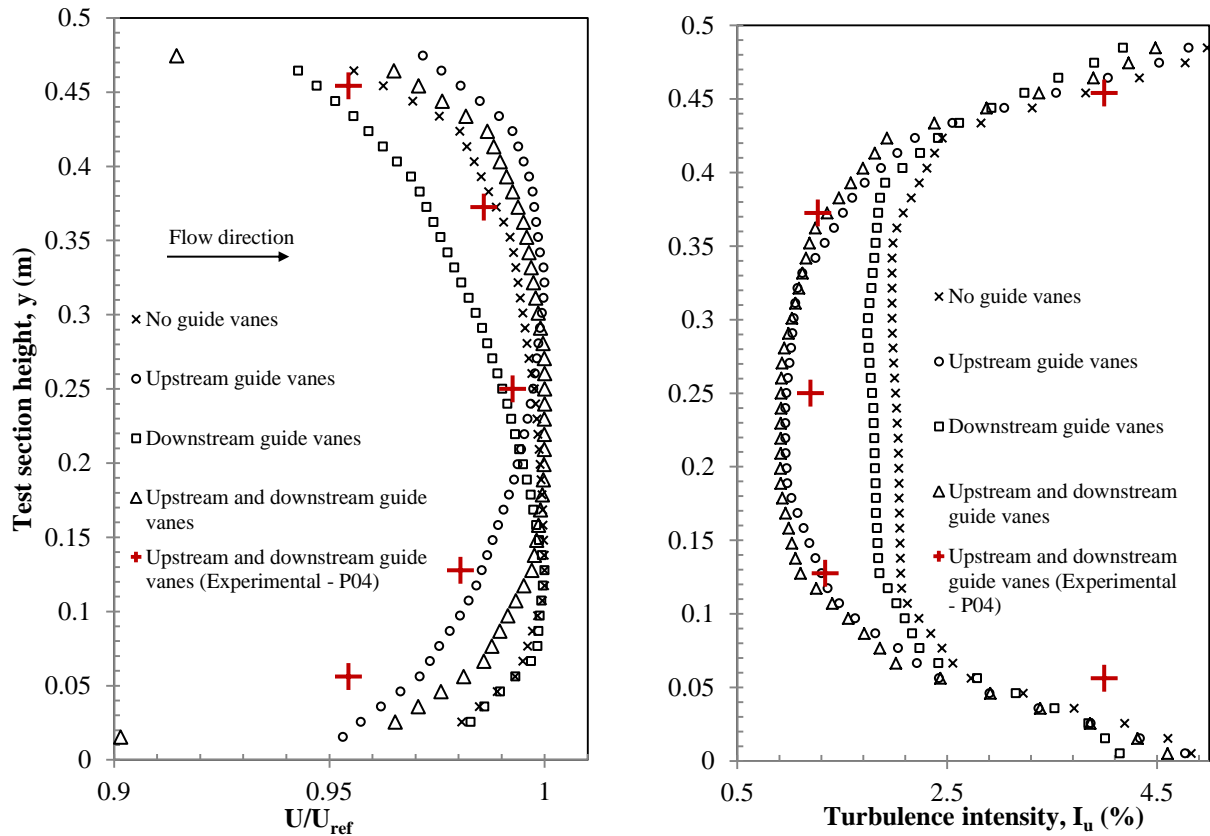
Figure 10 Comparison between the dimensionless mean velocity and turbulence intensity of the flow at the test section for the different wind tunnel configurations (**X = 0.75 m, P04**). Highlighted (**red**) data points show measured wind tunnel values.

6.1.4.2 Test section flow uniformity

Figure 11 shows a comparison between the numerical and experimental results for the uniformity coefficient. While for the bottom plane (Y = 0.25 m), the average error across the measurement points was 14 % with point P01 getting the maximum error . While for the top plane (Y = 0.125 m), the average error across the measurement points was 12% (abosule error of relative measure). Similarly, point P01 getting the maximum error. Average uniformity of 0.54 % was obtained from the middle section points and 0.48 % from the bottom section points.
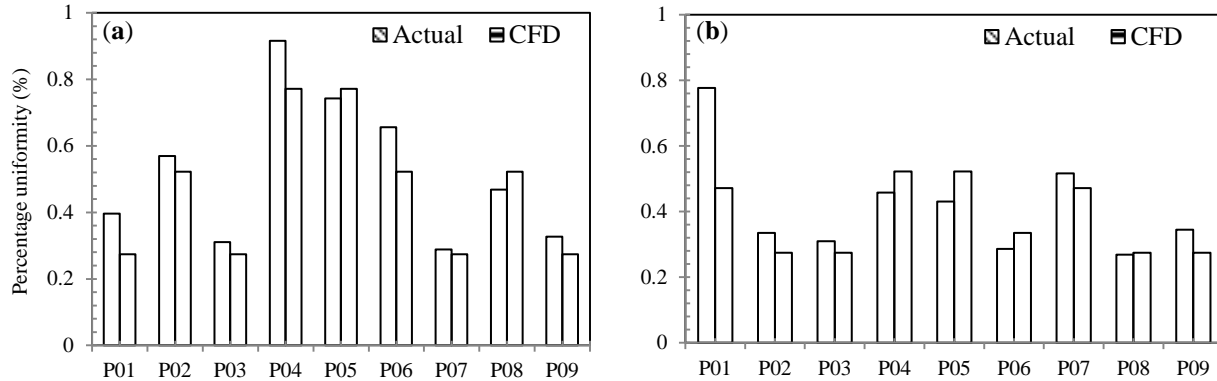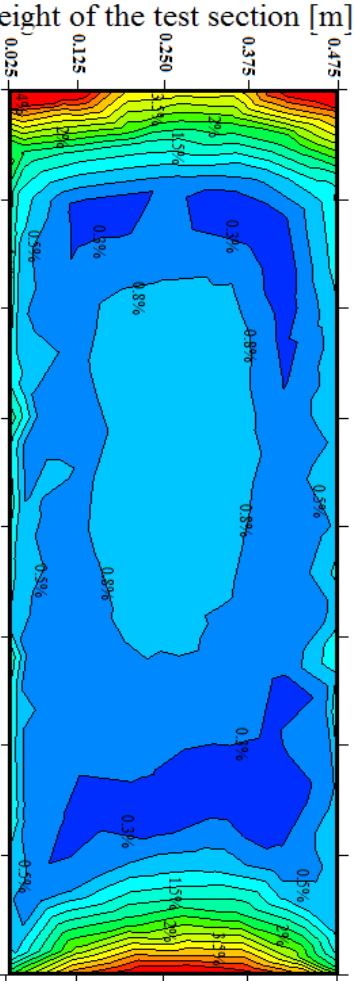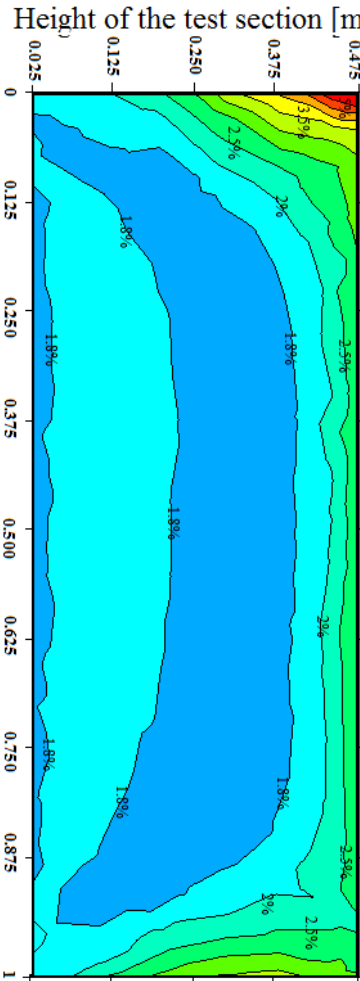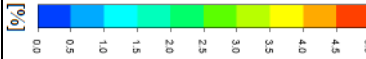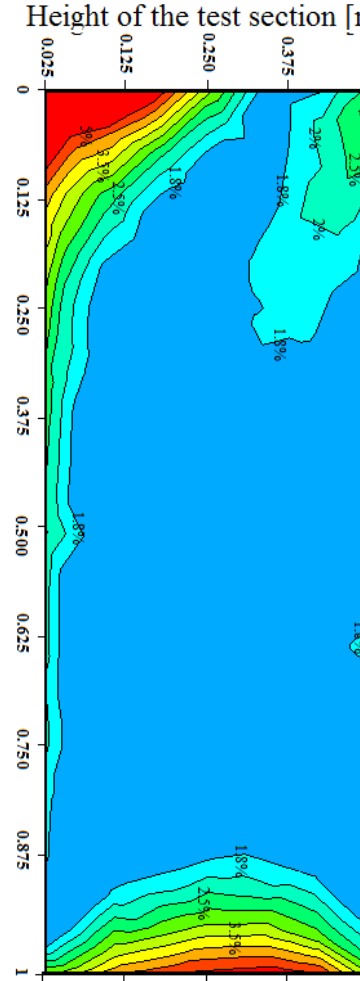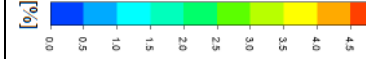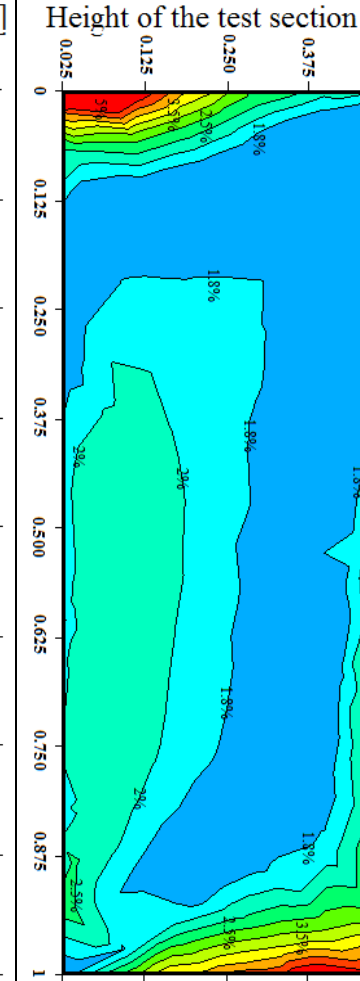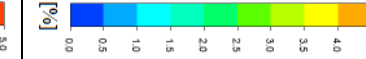
Figure 11 Comparison of the CFD and experimental results (P01 – P09) for the percentage uniformity of flow at: (a) Y = 0.25 m and (b) Y = 0.125 m (Configuration 4).

Table 9 summarises the flow uniformity results in the test section for the guide vane configurations. Note that the flow separations occurring near the walls were not included in this analysis hence, the top, bottom and side (0.025 m from wall) of the actual test section were not shown. Adding the guide vanes to the wind tunnel upstream corners improved the airflow uniformity by 36 % and combining upstream with downstream guide vanes improved the uniformity by 65 %. The situation with only downstream guide vane was worse than in the case of only upstream guide vanes, improving the uniformity by only 10 %. This clearly indicates that the quality of the flow in the test section was more affected by the flow condition in the upstream section than the downstream section. Hence, special attention must be given while designing the guide vane at the upstream corners particularly the section in line with the test section.

Table 9 Percentage uniformity of flow in test section for the different guide vane configurations

(g) Upstream and downstream	(c) Downstream guide vanes	(f) Upstream guide vanes	(e) No guide vanes	Horizontal cross section (Z = 0.25 m)
Average speed: **15.85 m/s** Uniformity: **0.51 % (CFD)** Uniformity: **0.66 % (Actual)**	Average speed: **16.07 m/s** Average uniformity: **1.28 %**	Average speed: **15.97 m/s** Average uniformity: **0.92 %**	Average speed: **16.27 m/s** Average uniformity: **1.44 %**	Data

21

6.1.4.3 Test section flow angularity

Figure 12 shows the flow angularity variation across the test section height for different guide vane configurations. The flow angularity was measured at three different test section height; bottom, center and top at the mean wind speed of 15.65 m/s. The measurements revealed a slight increase in the angularity of the flow near the test section roof and floor.
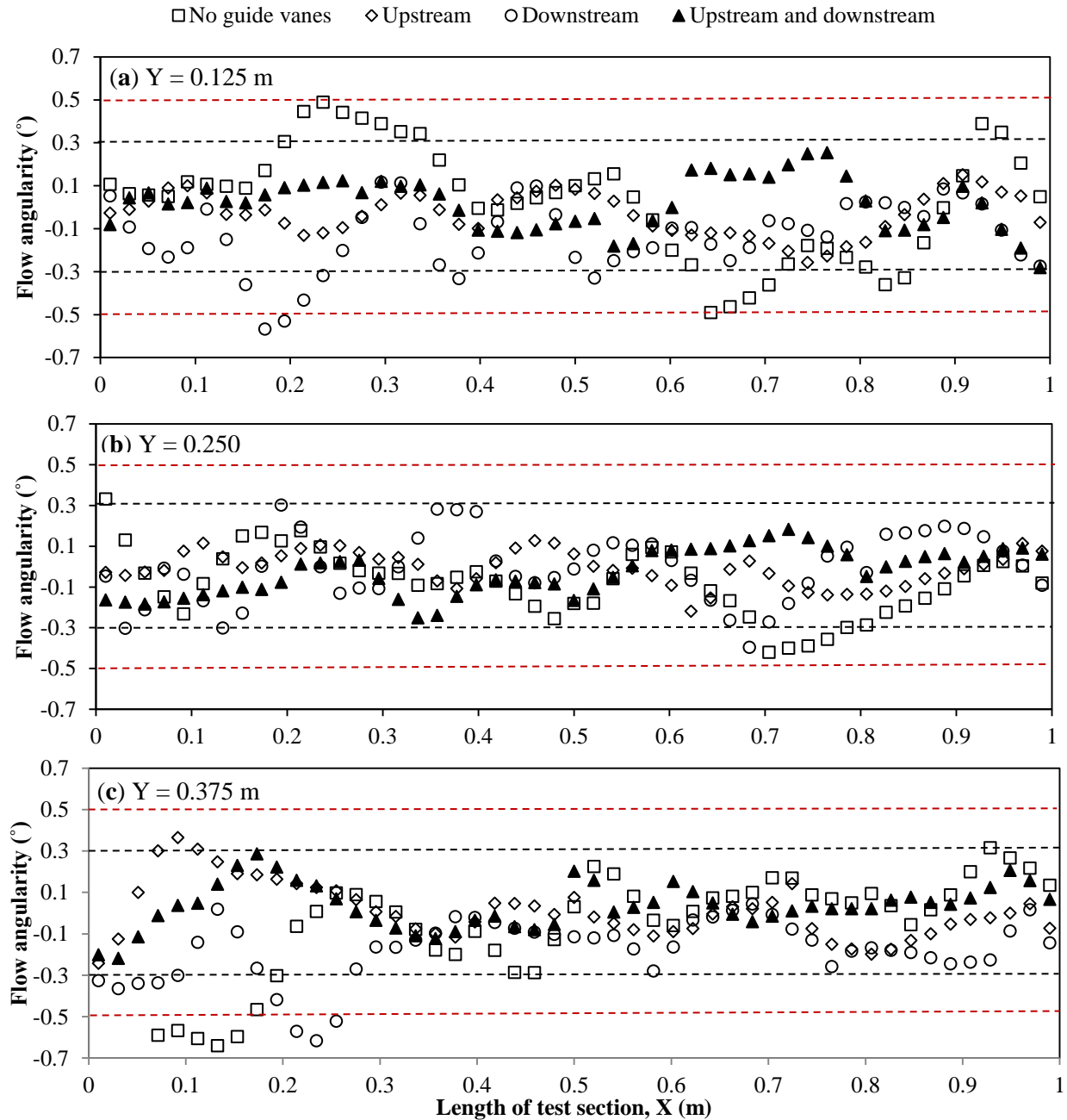
Figure 12 Flow angularity variation across the test section for different guide vane configurations: (a) X = 0.125 m, (b) Y = 0.250 m and (c) Y = 0.375 m. Red dotted line at $\pm\,0.5°$ and black dotted line at $\pm\,0.3°$.

It can be observed that the flow angularity for the first (no guide vanes) and third configuration (downstream) went above 0.5˚ particularly near the entrance and exit of the test section, while the second configuration with the upstream guide vanes maintained the flow angularity below 0.5˚ and the combined upstream and downstream below 0.3˚.

6.1.4.4 Dynamic pressure distribution

The dynamic pressure was measured at the test section axial position corresponding to the location of the Pitot - static tube (P01 – P09). Good agreement was obtained. The error was less than 10% between actual and CFD results (Figure 13).
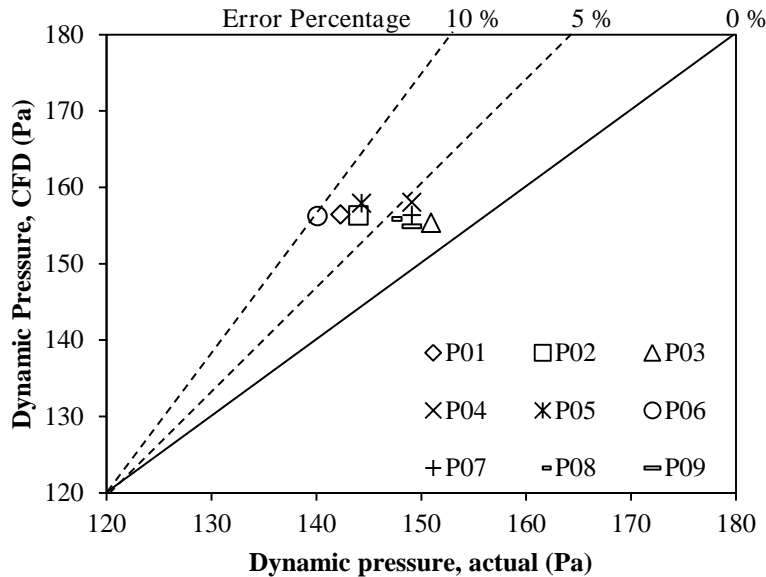
Figure 13 Comparison between measured and CFD results for dynamic pressure. Dotted lines indicate error percentages.

6.2 Wind tunnel test section with block model

Figure 14 shows the velocity contour of a vertical and horizontal cross sectional plane in the wind tunnel with the block model. A symmetric wind profile was observed before the test section and non-uniform profile at the exit due to the blockage of the test block model. A uniform air flow enters the test section inlet with the flow splitting at the front side of the block shearing across the top and side surfaces and exiting to the diffuser section. Existence of flow separation and wake regions were seen at the leeward side of the block model.

Table 10 summarises the measured and CFD values of the dimensionless mean velocity at points A – G in the X, Y and Z direction. The flow speed values were made dimensionless by division by a reference wind speed, which was the measured wind speeds at point A (mean).
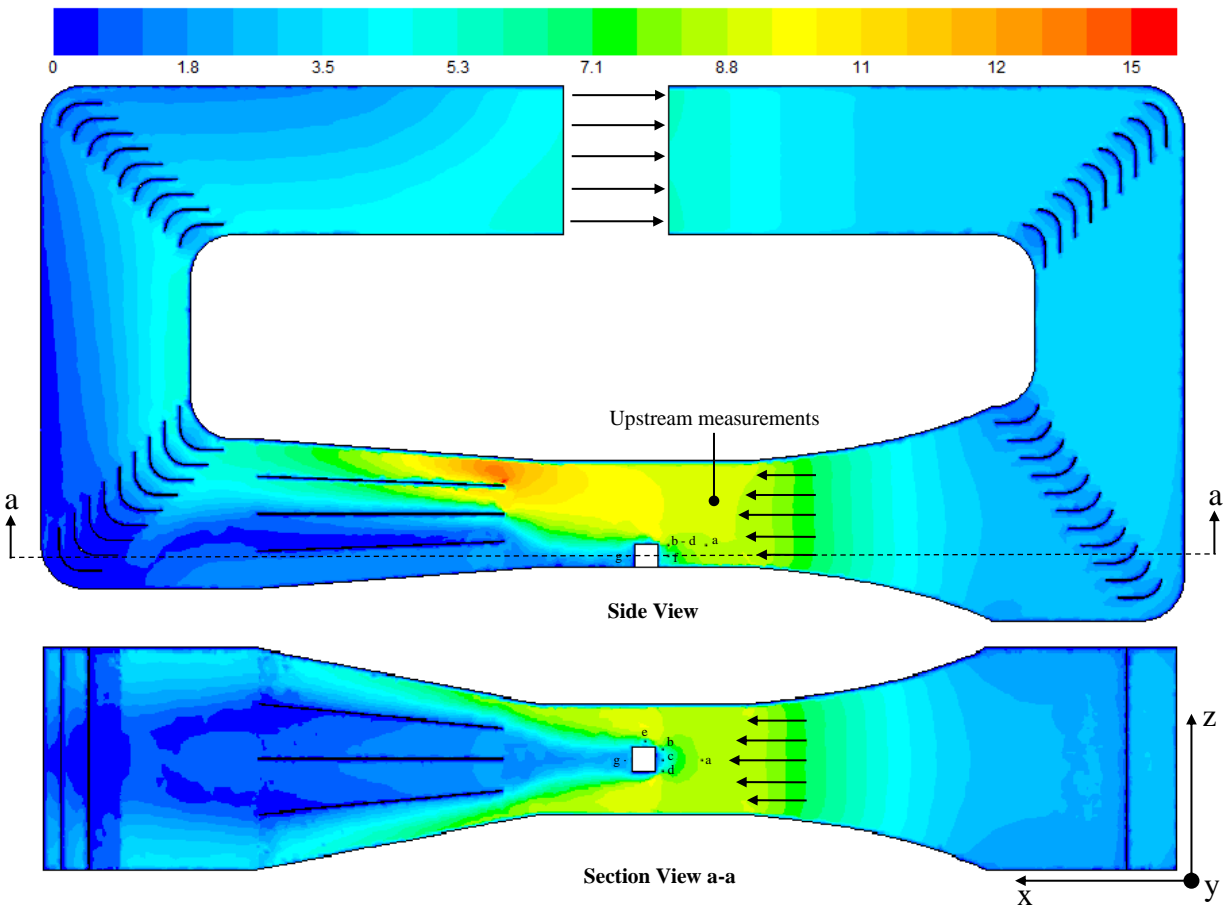
Figure 14 Contours of velocity magnitude inside the wind tunnel with block test model.

Table 10 Comparison between measured and CFD results for mean velocity at points A - G (X, Y, Z) (stream wise, vertical and lateral) around the test block model.
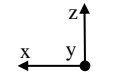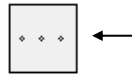
Points		$U_{X\ actual}$ dimensionless	$U_{Y\ actual}$ dimensionless	$U_{Z\ actual}$ dimensionless	$U_{X\ CFD}$ dimensionless	$U_{Y\ CFD}$ dimensionless	$U_{Z\ CFD}$ dimensionless
A		**1.00**	**0.04**	**-0.02**	1.01	0.05	-0.02
B		0.92	0.10	0.32	0.88	0.11	0.29
C		0.71	0.18	-0.10	0.68	0.14	-0.09
D		0.91	0.10	-0.32	0.90	0.11	-0.29
E		0.93	0.09	0.07	0.87	0.11	0.06
F		0.36	0.05	-0.05	0.32	0.05	-0.04
G		0.40	0.03	0.04	0.32	0.02	0.04

24

Figure 15 shows the comparison between the measured and CFD values for the turbulence intensity for points A – G around the block type model. Highest level of turbulence was observed for point E (side), F (front) and G (back). The CFD results were consistent with the experimental data; with all the measurement points error below 10% except for point B and G which were slightly above 10%.
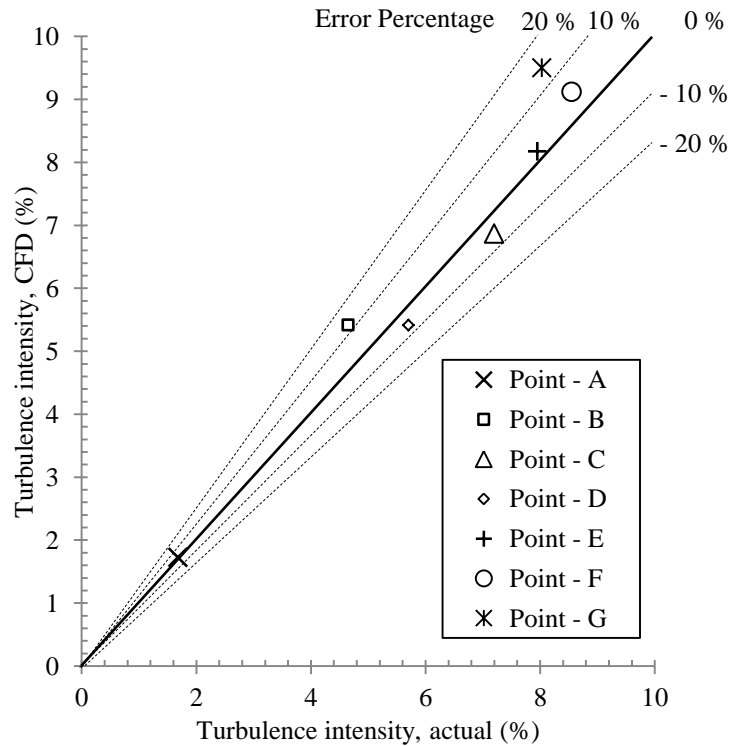

Figure 15 Comparison between the measured and CFD values for the turbulence intensity for points A – G around the block model. Dotted lines indicate the error percentage.

Figure 16 shows the measured and CFD values for the pressure coefficients at the front, back, left, right and top surfaces of the block model. As expected the points located at the front surface experience the maximum value, and with the moving air stream towards the top, right and left side, the pressure coefficient decreases, indicating the acceleration of the flow. The measured pressure coefficient along the right and left surface of the block were very close, indicating the flow symmetry for the zero incident angle wind. In point P1 – Top, the pressure coefficient drop sharply. This point was at the front edge of the top surface where flow separation occurs. While for the back side of the of the block model, a uniform pressure distribution was observed. This was because of the separation of the air stream from the sides; an almost uniform low pressure wake was formed around the back surface. CFD and experimental results showed good agreement, with the error below 10% except for point P1 - left which seem to be sensitive to the angle of attack. Measurements at the front surface of the block gave the highest accuracy with average error of only 2% between the points.
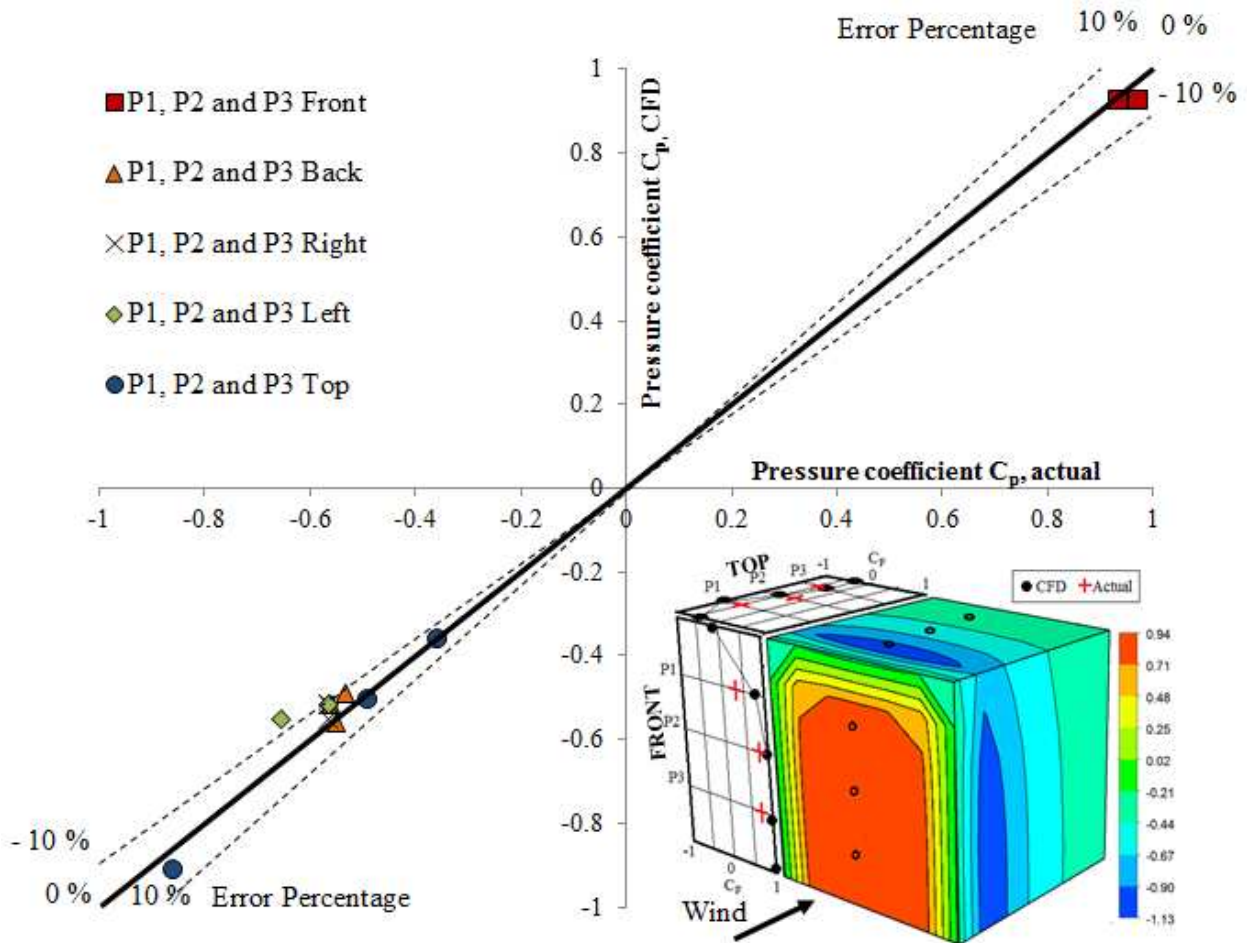
25

Figure 16 Comparison between CFD and experimental values for surface pressure coefficients around the block model. Dotted lines represent 10 % error percentage.

6.3 Comparison of turbulence models

The present study depicts the most suitable turbulence model for designing a closed-loop subsonic wind tunnel. Figure 17 shows the comparison between different turbulence models results for test section flow speeds and turbulence intensity. The CFD result for the calculated velocity showed relatively small variations for the turbulence models compared with the experimental data (within the range of 5 - 10 % error). The analysis shows that the k-epsilon and k-omega standard models closely predicted the flow speed (3 and 4 % error) and turbulence intensity (7 and 10 % error). While the Reynolds-Stress Model over predicted the velocity results by up to 7 % (Linear Pressure-Strain) and 10% (Stress-Omega).
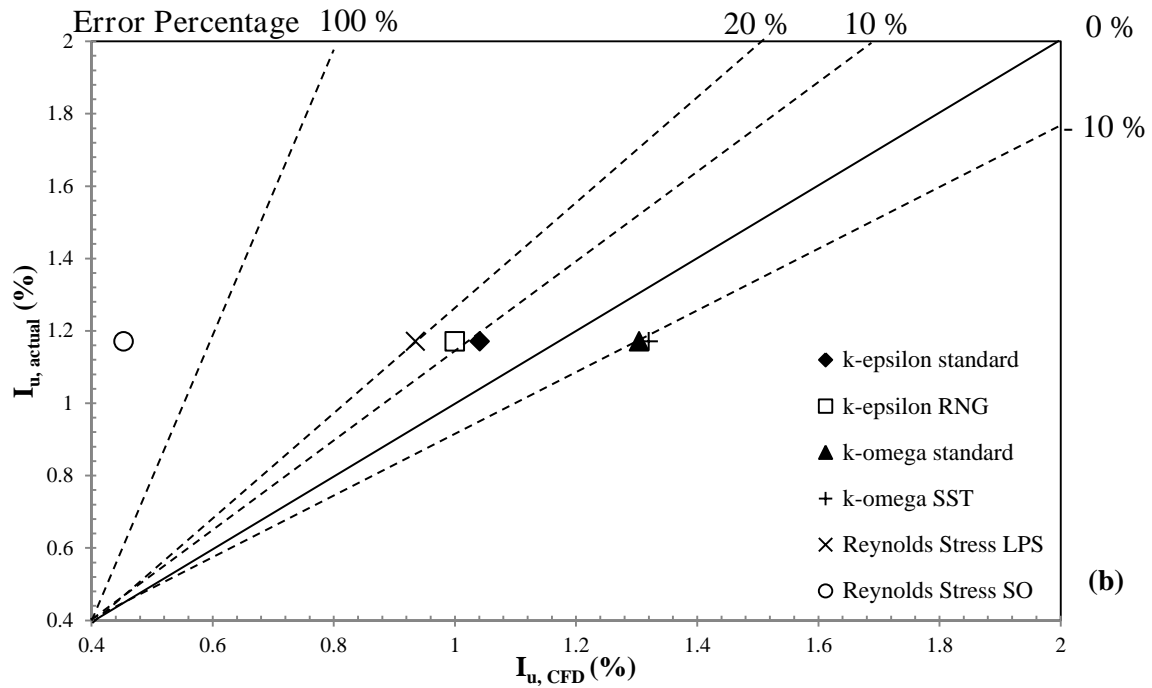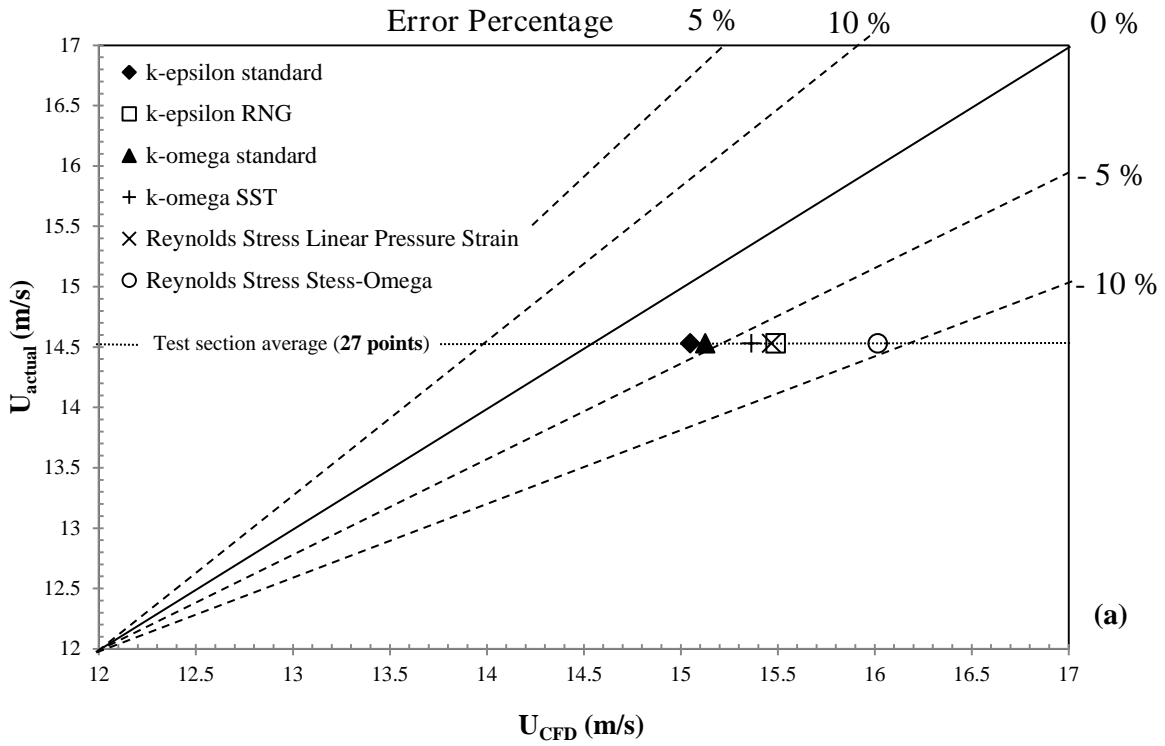
Figure 17 (a) Comparison between the test section flow speeds for different turbulence models. (b) comparison between the test section flow turbulence intensity for different turbulence models.

7. CONCLUSION

A numerical investigation into the design and simulation of the flow parameters in a closed-loop subsonic wind tunnel was carried out by incorporating Computational Fluid Dynamics (CFD). An analytical pressure loss model to determine the required intake fan pressure was established. A uniform boundary condition of the calculated pressure was imposed along the inlet surface (intake fan) and the pressure outlet was set to zero gauge pressure. A full-scale CFD model of the entire wind tunnel was considered instead of the conventional approach. This allowed for the optimisation of the flow quality not only in the test section but also the overall flow in other wind tunnel sections. The study developed a simpler approach to flow improvements by eliminating the flow separations in the corners by using guide vanes with extensions which will certainly improve the up-flow, cross-flow and turbulence in the test section.

Adding the guide vanes to the wind tunnel upstream corners improved the airflow uniformity by 36% and combining upstream with downstream guide vanes improved the uniformity by 65%. The situation with only downstream guide vane was worse than in the case of only upstream guide vanes, improving the uniformity by only 10%. This clearly indicates that the flow quality in the test section was greatly affected by the flow condition in the upstream section than the downstream section. Hence, special attention must be given while designing the guide vane at the upstream corners particularly the section in line with the test section. The addition of splitting plates at the diffuser section effectively reduced the velocity variations at diffuser exit from 30 to 5%.

Furthermore, the numerical model was validated for the case of an empty test section and for the case of which a block-type model was centrally located in the test section. The findings from experimental validation of the empty test section were found to be in good agreement with the computational results. Uniformity of flow mean speed and turbulence intensity levels were found to be in line with 1% between the measurement points with the flow angularity below 0.5°. The validation of the test section with the block model showed that the CFD can generally reproduce the wind tunnel measurements of mean velocities, pressure coefficients and turbulent intensities with an error below 10%.

The authors compared various CFD turbulent models and were evaluated against analytically and experimentally predicted velocity and turbulence values. The analysis shows that the k-epsilon and k-omega standard models closely predicted the test section flow speed (3 and 4% error) and turbulence intensity (7 and 10% error) and were concluded as the most suitable turbulence models for this study.

ACKNOWLEDGEMENT

REFERENCES

[1] Mehta R, Bradshaw P, Technical notes: Design rules for small low speed wind tunnels, The Aeronautical Journal of the Royal Aeronautical Society, 1979, 443-449.

[2] Cermak J, Wind tunnel design for physical modelling of atmospheric boundary layers, Journal of Engineering Mechanics, 1981, 107(3), 523-642.

[3] Barlow J, Rae W, Pope A, Low Speed Wind Tunnel Testing, John Wiley & Sons, 1999, 3, 105-122

[4] Kulkarni S, Minor M, Deaver M, Pardyjak E and Hollerbach J, Design, Sensing, and Control of a Scaled Wind Tunnel for Atmospheric Display, IEEE/ASME Transactions on Mechatronics, 2012, 17(4), 635-645.

[5] Ghani S, Aroussi A, Rice E, Simulation of road vehicle natural environment in a climatic wind tunnel, Simulation Practice and Theory, 2001, 8, 359-375.

[6] Launder B, Spalding D, Lectures in mathematical models of turbulence, Academic Press, 1972, 55.

[7] Gartmann A, Fister W, Schwanghart W Müller M, CFD modelling and validation of measured wind field data in portable wind tunnel, Aeolian Research, 2011, 3, 315-325.

[8] Moonen P, Blocken B, Roels S, Carmeliat J, Numerical modelling of the flow conditions in a closed-circuit low-speed wind tunnel, Journal of Wind Engineering and Industrial Aerodynamics, 2006, 94, 699-723.

[9] Gordon R, Imbabi M, CFD simulation and experimental validation of a new closed circuit wind/water tunnel design, Journal of Fluids Engineering, 1998, 120(2), 311-318.

[10] Moonen P, Blocken B, Carmeliat J, Indicators for the evaluation of wind tunnel test section flow quality and application to a numerical closed-circuit wind tunnel, Journal of Wind Engineering and Industrial Aerodynamics, 2007, 95, 1289-1314.

[11] Balendra T, Shah D, Tey K, Kong S, Evaluation of flow characteristics in the NUS-HDB Wind Tunnel, Journal of Wind Engineering and Industrial Aerodynamics, 2002, 90, 675-688.

[12] Diana G, De Ponte S, Falco M, Zasso A, A new large wind tunnel for civil-environmental and aeronautical applications, Journal of Wind Engineering and Industrial Aerodynamics, 1998, 74-76, 553-565.

[13] Li M, Liao H, Zheng S, A new extreme large boundary layer wind tunnel at Southwest Jiatong University, The Seventh Asia-Pacific Conference on Wind Engineering, November 8-12, 2009, Taipei, Taiwan.

[14] Wittwer A, Möller S, Characteristics of the low-speed wind tunnel of the UNNE, Journal of Wind Engineering and Industrial Aerodynamics, 2000, 84, 307-320.

[15] Nader G, Dos Santos C, Jabardo P, Cardoso M, Taira N, Pereira M, Characterization of low turbulence wind tunnel, Metrology for a Sustainable Development, September 17-22, 2006, Rio de Janeiro, Brazil.

[16] Sahin B, Ward-Smith A, Lane D, The pressure drop and flow characteristics of wide-angle screened diffusers of large area ratio, Journal of Wind Engineering, 1995, 58, 33-50.

[17] Gan G, Riffat S, Computational and experimental study of pressure losses in duct transitions, International Journal of Energy Research, 1998, 20, 979-987.

[18] Chen K, Jin X, Zhao J, Design and characteristics of a large boundary-layer wind tunnel with two test sections, The Seventh Asia-Pacific Conference on Wind Engineering, November 8-12, 2009, Taipei, Taiwan.

[19] Vlajina M, Design, construction and evaluation of a subsonic wind tunnel, Massachusetts Institute of Technology Department of Aeronautics and Astronautics, 1970, 17-20.

[20] You D, Mittal R, Wang M, Moin P, Analysis of stability and accuracy of finite-difference schemes on a skewed mesh, Journal of Computational Physics, 2006, 213, 184-204.

[21] FLUENT Incorporated: FLUENT user guide [Online] 2006, available from: www1.ansys.com (access date Feb 1, 2012).

[22] The Engineering Toolbox: Roughness and Surface Coefficients of Ventilation Ducts [Online] 2012, available from: http://www.engineeringtoolbox.com (access date Feb 1, 2012).

[23] Chung T, Computational fluid dynamics. Cambridge University Press, 2002, 1, 15-21.

[24] Calautit JK, Chaudhry HN, Hughes BR, Ghani SA, Comparison between evaporative cooling and a heat pipe assisted thermal loop for a commercial wind tower in hot and dry climatic conditions, 2013, 101, 740-755.

[25] Mehta U, Some aspects of uncertainty in computational fluid dynamics results. Journal of Fluids Engineering;1991, 113, 539–543.

[26] Owen F, Owen A, Measurement and assessment of wind tunnel flow quality, Progress in Aerospace Sciences, 2008, 44, 315-348.

[27] Watakabe M, Ohashi M, Okada H, Okuda Y, Kikitsu H, Ito S, Sasaki Y, Yasui K, Yoshikawa K, Tonagi M, Comparison of wind pressure measurements on tower-like structure obtained from full-scale observation, wind tunnel test, and the CFD technology, Journal of Wind Engineering and Industrial Aerodynamics, 2002, 90, 1817-1829.

[28] Chong T, Joseph P, Davies P, Design and Characterisation of a Quiet, Low Turbulence Open Jet Blow Down Wind Tunnel in ISVR, ISVR Technical Report NO 322 University of Southampton, 2008.

[29] Montazeri H, Azizian R, Experimental study on natural ventilation performance of one-sided wind catcher, Building and Environment, 2008, 43 2193–2202.

[30] Esfeh M, Dehghan A, Manshadi M, Mohagheghian S, Visualized flow structure around and inside of one-sided wind-catchers, Energy and Buildings, 2012, 55, 545-552.

[31] Calautit JK, Hughes BR, Ghani SA, Numerical investigation of the integration of heat transfer devices into wind towers, Chemical Engineering Transactions, 2013, 34, 43-48.